Wettability and Anti-Corrosion Performances of Carbon Nanotube-Silane Composite Coatings

Luigi Calabrese [1,2,*] **, Amani Khaskoussi** [2] **and Edoardo Proverbio** [1,2]

[1] Department of Engineering, University of Messina, Contrada di Dio, 98166 Messina, Italy; eproverbio@unime.it

[2] National Interuniversity Consortium of Materials Science and Technology, INSTM, Via Giuseppe Giusti 9, 50121 Firenze, Italy; khaskhoussiamani105@gmail.com

[*] Correspondence: lcalabrese@unime.it

check for updates

Abstract: In this paper, a sol-gel N-propyl-trimethoxy-silane coating filled with different amount of multi-wall carbon nanotubes (MWCNTs) was investigated in order to improve the aluminum corrosion resistance. The nanocomposite coating was applied, by drop casting, on AA6061 aluminum alloy substrate. The morphological analysis highlighted that a uniform sol-gel coating was obtained with 0.4 wt.% CNT. Lower or higher nanotube contents lead to the formation of heterogeneities or agglomeration in the coating, respectively. Furthermore, all nanocomposite coatings exhibited effective adhesion to the substrate. In particular, the pull-off strength ranged in 0.82–1.17 MPa. Corrosion protection of the aluminum alloy in NaCl 3.5 wt.% electrolyte (seawater) was significantly improved after CNT addition to the base coating. The stability in electrochemical impedance was observed during three days of immersion in the sodium chloride solution. AS3-CNT2 and AS3-CNT4 batches showed advanced electrochemical stability during immersion tests. Furthermore, interesting results were evidenced in potentiodynamic polarization curves where a decrease of the corrosion current of at least two order of magnitude was observed. Moreover, the breakdown potential was shifted toward noble values. Best results were observed on AS3-CNT6 specimen which exhibited a passivation current density of approximately 1.0×10^{-5} mA/cm^2 and a breaking potential of 0.620 V/AgAgCl$_{sat}$.

Keywords: silane; carbon nanotube; coating; corrosion; superhydrophobicity

1. Introduction

Organic coatings are widely used to protect metals and alloys from corrosion. In order to extend their service life and to reduce their maintaining costs, these protective coatings should maintain their mechanical and barrier properties during time in critical environmental conditions.

Although, because of a progressive water diffusion through the coating bulk, a gradual depletion of anti-corrosion capability and adhesion with the substrate occur, which leads to a significant reduction of protective action, increasing consequently the damage risks related to local corrosion phenomena [1].

In order to overcome this issue, a recent and promising approach focuses on the application of superhydrophobic composite coatings (SHCs) in order to avoid corrosion phenomena triggering at the metals/alloys surface [2].

The purpose is to modify the surface wettability aiming to delay the water diffusion in the coating by reducing significantly its interaction with water. The water contact angle (WCA) can be considered a basic index of the surface wetting properties. Furthermore, the sliding angle (SA) can be considered as a benefit in order to discriminate the high performing surfaces. Depending on the contact angle value the surface can have hydrophilic (WCA < 90°), hydrophobic (WCA > 90°), or superhydrophobic

(WCA > 150° and SA < 5°) behavior [3]. In order to enhance the superhydrophobic characteristics of the surface, some techniques are based on the use of micro and nano hierarchical structures/filler [4–6] or by using a chemical with low surface energy and protective capabilities [7–10] can be adopted.

In the recent years, nano-filler-based composites (e.g., oxides [11–13] or CNT [14,15] based) are, among all, the most promising composites in terms of application effectiveness. The research contexts for the use of SHC are manifold such as, self-cleaning, anti-icing, or not least anticorrosive coatings [16–18].

Different polymer matrices were loaded with carbonaceous fillers (CNT, graphite, graphene, and carbon black) in order to improve the corrosion resistance [19–24].

De Nicola and coworkers [25] showed that CNT films, obtained by chemical vapor deposition on stainless steel substrate, improved the hydrophobic behavior (WCA equal to 154°) of the substrate indicating relevant applications in corrosion and fouling prevention.

Zhu et al. [26] investigated a multiwall carbon nanotube (MWCNT)-Co carbon-based film, obtained by electrochemical deposition technology, evidencing very promising results in terms of corrosion prevention and durability. Analogously, Zhou et al. [27] confirmed these effective results also by using MWCNT-Ni coatings on stainless steel support.

In addition, carbon nanotubes coatings were used in several applications because of their unique mechanical, structural thermal and electrical properties [28]. The CNT-doped composites showed promising fatigue resistance and CNTs have been utilized as chemical sensors, hydrogen storage materials, and electrodes [29]. Moreover, CNTs have been also added into polyaniline coating to decrease its corrosive solution or permeability for oxygen [30]. In order to increase the adhesion between the coatings and the metals, the CNT have been incorporated into epoxy coating to increase adhesion and cohesion between coatings and metal substrates [31].

The use of silane as matrix in the composite coating preparation could be a suitable option in order to enhance the anti-corrosion performances and stability of CNT-based coatings.

It can improve the chemical interaction to CNT filler surface contributing to improve the corrosion protection of the composite coating [32,33]. In addition, using the silane as a matrix for the fabrication of CNT coatings can enhance their performances and the dispersion of CNTs.

Bis-[triethoxysilylpropyl] tetrasulfide (BTESPT) silane film modified with MWCNT was applied on stainless steel substrate in [33] highlighting successful results. In particular, the filled silane coating exhibited a low frequency amplitude three order of magnitude higher than bare stainless steel surface, confirming the suitable barrier action of the proposed silane-CNT coating.

Jeeva Jothi and Palanivelu [34] proposed to apply different filler (cloisite 15A, MWCNT and cerium chloride) on a sol-gel silane coating, prepared by using 3-glycidoxypropyltrimethoxysilane (GPTMS), and octyltriethoxysilane (OTES). The results evidenced a beneficial effect on the mobilization of the corrosion potential and a slight improvement on the corrosion current due to the filler addition.

Montemor et al. [35] assessed the corrosion behavior of AZ31 magnesium alloy (Mg AZ31) coated with a bis-aminosilane film filled with MWCNT. The electrochemical results highlighted that the CNT-based composite coatings are homogenous and are able to significantly delay the corrosion activation phenomena on AZ31 magnesium alloy. These results were furthermore improved doping the CNT filler with a rare-earth salt that contributes to delay the onset of corrosion activity.

Recently, Nezamdoust et al. [36] investigated a composite coating constituted by phenyl-trimethoxysilane (PTMS) matrix and hydroxylated multi-walled carbon nanotubes as reinforcement at varying filler content in order to enhance the corrosion protection capability. The coatings were deposited on AM60B magnesium alloy by dip-coating. Although the hydrophobic properties were not relevant, the corrosion resistance of the PTMS film was considerably increased because of the addition of 500 ppm of CNT filler.

These results indicate that CNT-silane composite coatings may be a promising option for increasing the short and medium term durability of metal alloys. This could allow improving the management of

storage, handling and life services of their components with beneficial effects in terms of manufacturing and maintaining costs.

In this concern, aim of this paper is to assess the wettability and anti-corrosion performances of a sol-gel silane film filled with MWCNT for critical environmental conditions (such as marine application). Different amount of filler content were used in order to study their contribution in the corrosion protection performances. The effect of the addition of different amount of carbon nano-tubes in the silane film was investigated coupling sessile drop, adhesion, and electrochemical analysis. In particular potentiodynamic and electrochemical impedance spectroscopy (EIS) measurements were performed at varying immersion time in 3.5 wt.% NaCl solution in order to evaluate the coating stability and protection during time.

2. Materials and Methods

2.1. Carbon Nanotube Synthesis

Not functionalized carbon nanotubes (CNT) were prepared based on the synthesis procedure reported in [37]. In particular, the CNT synthesis has been performed by chemical vapor deposition (CVD) under continuous flow, at 120 cc/min, in 1:1 i-C_4H_{10}:H_2. The synthesized product was purified by using a 1 M NaOH solution (at 80 °C) and then by a 37 wt.% HCl solution (at 25 °C) [38]. The obtained product consisted in multi walled carbon nanotubes (MWCNT). The CNT surface area is 196 m^2/g. Surface areas (m^2/g) was determined by adsorption-desorption of dinitrogen at 77 K, after the samples had been outgassed (10^{-4} mbar) at 353 K for 2 h, using Qsurf Series surface area analyzers. The SEM images of the MWCNT is reported in [39].

2.2. Coating Synthesis

N-propyl-trimethoxy-silane, S3 (supplied by Sigma Aldrich, St. Louis, MO, USA) was used as film matrix. The silane solution was prepared by dissolving 10 vol.% of silane compound in a mixture of ethanol (10 vol.%) and 80 vol.% of bi-distilled water. The pH of the silane solutions was adjusted to values around 4.2 using acetic acid. The solution rests under magnetic stirring at 25 °C, for 24 h in order to complete the silane hydrolysis. Afterword, the CNT filler at different percentages (0.2 wt.%, 0.4 wt.% and 0.6 wt.%) were added in the hydrolyzed silane solution. The composite solution was sonicated for 2 h followed by additional magnetic stirring for 1 h. For comparative purposes silane solutions, without CNT addition was also realized. This silane was chosen because of its dispersive ability of CNTs. In addition this silane is known by its good adhesion property, environmental friendly property, and adequate corrosion inhibition [40].

Metal support with shape 20 × 40 × 0.5 mm were cut from a commercial aluminum 6061 sheet. Preliminary, all samples were mechanically polished with emery paper (grade 800), cleaned in a 0.1 N NaOH solution for 60 s, washed in bi-distilled water and eventually with ethanol.

The coating deposition was obtained by drop-casting of composite slurry on the pre-treated aluminum samples. After a soft drying at room temperature open to air for 5 min, the coated samples were cured in an oven at 80 °C for 12 h. The thickness of the composite coatings was about 20–30 μm for all batches. Figure 1 summarizes the coating preparation set-up.

Details of the different synthesized coating, clarifying sample codes, filler content, and coating specification, are given in Table 1. In particular, samples were coded with a prefix AS3 indicating the presence of a silane layer on the aluminum surface. For carbon nanotube based silane coatings a "-CNT" suffix was furthermore added. The final number codifies the amount of filler added in the formulation.
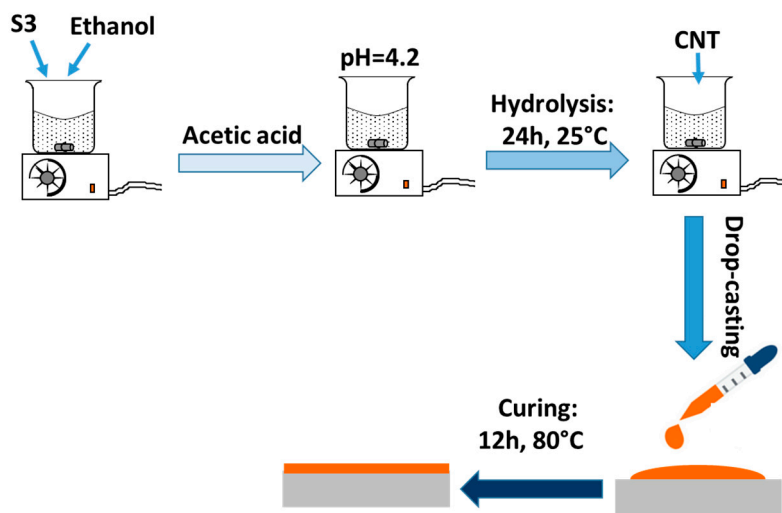
Figure 1. Scheme of the four step carbon nanotubes (CNT) coating process deposition.

Table 1. Samples summary. Sample codes, filler content, matrix, and coating specification.

Code	CNT wt.%	Silane	Notes
Al	-	-	Bare aluminum
AS3	-	S3	Silane coating
AS3-CNT2	0.2	S3	Composite coating
AS3-CNT4	0.4	S3	Composite coating
AS3-CNT6	0.6	S3	Composite coating

2.3. Experimental Analysis

Water contact angle measurements were carried out by using a tensiometer equipment (Attension Theta by Biolin Scientific, Gothenburg, Sweden). A distilled water droplet (volume 1 μL) was gently placed on the coating surfaces at room temperature (25 °C). The droplet profile was acquired by a micro CCD camera automatically analyzed by the instrument software. For each sample, 50 measurements (placed in order to obtain a regular grid on the surface) were carried out for all samples.

Morphological analysis of the surface features was carried out using a focused ion dual beam/scanning electron microscope (FIB-SEM ZEISS Crossbeam 540, ZEISS, Obwerkochen, Germany).

In order to evaluate the coating adhesion on the substrate, the pull-off and tape peel tests were carried out.

The tape peel test, according to method B in ASTM D3359 standard, was performed realizing a cross-cut grid with six cuts (about 20 mm long) in each direction. Each cut was spaced about 2 mm apart. Then, an adhesive tape was applied over the cross-cut grid and accurately pressed with a pencil eraser. The tape was removed and the amount of detached coated area was rated. The detached grid area was evaluated according to the ASTM specifications, from 0B (low adhesion) to 5B (high adhesion) to quantitatively indicate the effectiveness of the interfacial adhesion between the coating and the substrate.

The pull-off adhesion test was carried out, according to the ASTM D4541 standard, by fixing, with an epoxy adhesive, a loading fixture to the coating surface. After adhesive drying, a portable testing equipment (Positest AT-M by Defelsko, Ogdensburg, NY, USA) was mounted at the loading fixture to progressively apply a normal stress to the sample surface. The failure stress was recorded when coating detachment occurred.

Potentiodynamic polarization and electrochemical impedance spectroscopy (EIS) tests were performed by using a SP-300 potentiostat (Biologic, Seyssinet-Pariset, France), equipped with a high sensitivity low current module. A conventional three-electrode cell was used: The coated sample is the

working electrode; a helicoid shaped platinum wire was used as the counter electrode. As the reference electrode, a saturated Ag/AgCl electrode probe was used. All tests were performed in 3.5 wt.% NaCl solution at room temperature and open to air conditions. The testing area was about 0.50 cm^2.

The potentiodynamic polarization measurements were performed, according to ISO 17475 standard, acquiring two separated anodic and cathodic polarization curves starting from the open circuit potential (OCP). A potential range ±1500 mV versus open circuit potential with a scanning rate of 1 mV/s was carried out. The EIS tests were carried out at open circuit potential (OCP) with a voltage amplitude of 10 mV and a frequency range from 0.05 mHz to 100 kHz (10 point for decade). Three replicas for each batch were performed.

3. Results and Discussion

3.1. Morphology

Preliminarily, a surface morphology evaluation was carried out on all composite batches. Figure 2 shows the top-view micrographs of CNT-silane composite film.
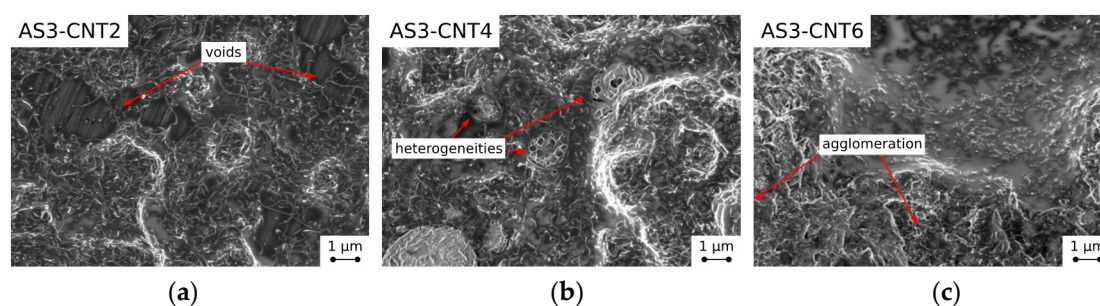

Figure 2. Top-view SEM images of CNT-silane composite film (**a**) AS3-CNT2; (**b**) AS3-CNT4; (**c**) AS3-CNT6.

The surface morphology of the coating with the lowest amount of CNT filler, AS3-CNT2, displays a not regular structure, Figure 2a. Some areas with large colonies of CNT filler can be indeed observed. At the same time, some cavities with smooth surface due to a local filler void can be furthermore identified, confirming the heterogeneous distribution of the coating. By improving the CNT content (AS3-CNT4 in Figure 2b), a uniform morphology with the CNT nanofiller in the form of well-distributed aggregates has been obtained. The surface profile is characterized by several peaks and valleys, because of the constituents' solidifications during the curing. However, the surface is homogeneously coated by the composite film. Some hemispherical heterogeneities are observed randomly located on the sample. These can be ascribed to the improper local ethanol evaporation during the curing step due to the slight higher viscosity of the composite slurry (considering the higher amount of nano-filler) compared to AS3-CNT2 batch. Eventually, the batch with highest amount of CNT, AS3-CNT6 in Figure 2c, showed an interconnected structure with CNT wires randomly tangled with the silane matrix. Some large agglomeration areas are also observed, where large entanglements occurred. Although the coating is without macro-cracks or defects indicating an appropriate adhesion between filler and silane matrix.

3.2. Wettability

The Figure 3 shows the water contact angle (WCA) of silane-based coatings at increasing CNT filler content. Bare aluminum WCA was also added as reference (dotted red line). The AS3 samples, unfilled silane coating, exhibit a higher WCA than the bare aluminum one. In particular, the water wettability increased form ~60° to ~90° confirming the beneficial effect of the presence of the silane layer on the surface hydrophobic behavior. Nevertheless, the composite coatings show a marked hydrophobic behavior, which becomes more evident with the increasing content of the carbonaceous

filler. The specimens with 0.4 wt.% and 0.6 wt.% of CNT filler reached WCA above 150° thus indicating an acquired superhydrophobic behavior of the surface. In particular, AS3-CNT6 batch showed the highest contact angle equal to 160.3°.
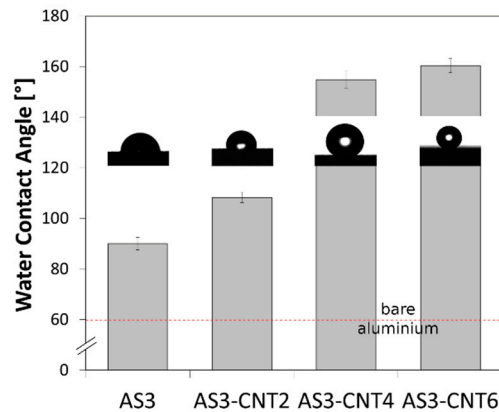

Figure 3. Water contact angle of silane-based coatings at increasing CNT filler content (Five replicates for each sample). Bare aluminum was added as reference (dotted red line).

This implies that water absorption could be severely limited in the composite coatings, resulting in a suitable durability in wet and humid environments in which the electrolyte surface interaction plays a relevant role in triggering surface corrosion phenomena [41].

3.3. Adhesion

The detached area (in percentage) observed after tape peel test for all composite coatings is reported in Figure 4. The amount of detached area is significantly influenced by the CNT filler content in the composite coating formulation. In particular, the AS3-CNT6 sample exhibits the lowest adhesion capability, evidencing a 9.3% of detached area (adhesion scale 3B according to ASTM D3359 standard). Instead, the batch with the lowest filler content (AS3-CNT2) did not show any detachment (adhesion scale 5B). The AS3-CNT4 showed intermediate adhesive properties with a detached area of 4.9% (adhesion scale 2B).
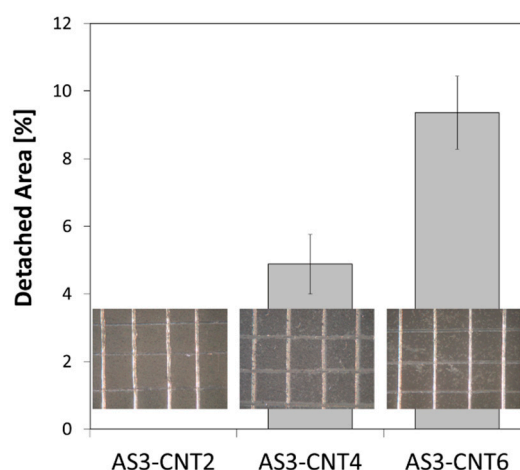

Figure 4. Detached area, observed after tape peel test, of silane-based coatings at increasing CNT filler content (three replicates for each coating).

The different adhesive properties among composite coatings can be attributed to the variation of the interfacial bond (i) between the coating and the aluminum support and (ii) between the nanotubes reinforcement and the silane matrix.

In fact, the silane matrix has trifunctional Si-OH hydroxyl groups, which confer a suitable chemical activity to the molecule. In particular, the silanol groups of the silane compound are able to react with the hydroxyl groups present on the aluminum surface, allowing the formation of Si-O-Al bonds, which significantly increase the adhesive properties at the composite/substrate interface [40]. Similarly, silane groups can also interact with the surface defects of carbon nanotubes in which carboxylic groups are present, leading to the consequent formation of silane-CNT filler covalent bond [32].

A high CNT content leads to a significant increase in the surface area of the reinforcement in the composite coating. Since the matrix must embed the filler, the unreacted silane groups capable of promoting the stiffening of the structure (e.g., crosslinking) are less frequent. The consequence is a reduction in the cohesive and adhesive properties of the composite coating for high CNT contents.

Even if the tape peel test is a suitable approach to qualitatively assess the adhesion capabilities of the composite coating, a further improvement of knowledge on adhesion performances can be acquired by performing pull-off tensile test, obtaining a quantitative evaluation of the adhesion/cohesion strength of the CNT-based layer.

Figure 5 summarizes the pull-off strength of silane-based coatings at increasing CNT filler content. All samples exhibit an adhesion strength higher than 0.80 MPa. As in tape peel test, the addition of low carbon nanotube filler (AS3-CNT2 sample) leads to a tensile adhesion strength about 30% higher than AS3-CNT6 one (characterized by 0.6 wt.% of CNT filler). In addition, the AS3-CNT2 evidenced a very relevant adhesion without coating detachment during pull-off test (Figure 4). This behavior is consistent with the more effective interaction between the silane matrix and the carbon nanotube filler in AS3-CNT2 sample. Hence, a higher stress level needs to be exceeded to trigger crack propagation and cohesive fracture [42].
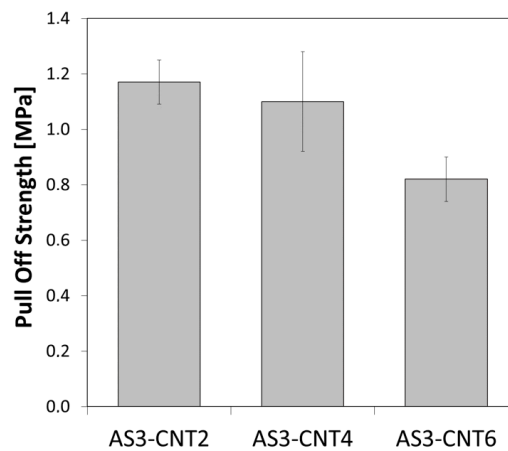

Figure 5. Pull-off strength of silane based coatings at increasing CNT filler content (three replicates for each coating).

These results indicate that the composite coating reached a high matrix crosslinking level. The CNT samples hydrophobic properties, shown in Figure 3, indicate a low interaction with the polar groups of the water. Consequently, the sol-gel layer reached a significant level of crosslinking and the polar silanol groups had the opportunity to interact with the reinforcement, the support or each other, forming oxygen bridges [41]. As mentioned above, the high CNT content has, probably, limited the formation of crosslinks inducing a decrease in adhesive properties of approximately 30% compared to the sample containing the lowest CNT content.

3.4. Potentiodynamic Analysis

DC polarization tests were carried out in order to acquire information on the stability of the CNT composite coating at increasing electrochemical potential. In addition, the comparison of the

characteristic curves for the different coating batches can provide a preliminary assessment of their electrochemical and anti-corrosion behavior.

The potentiodynamic polarization curves of the different CNT composite coatings immersed in NaCl 3.5 wt.% solution are reported in Figure 6. Bare aluminum and pure silane coatings were also added as references. In particular, cathodic and anodic branches are compared in Figure 6a,b, respectively.
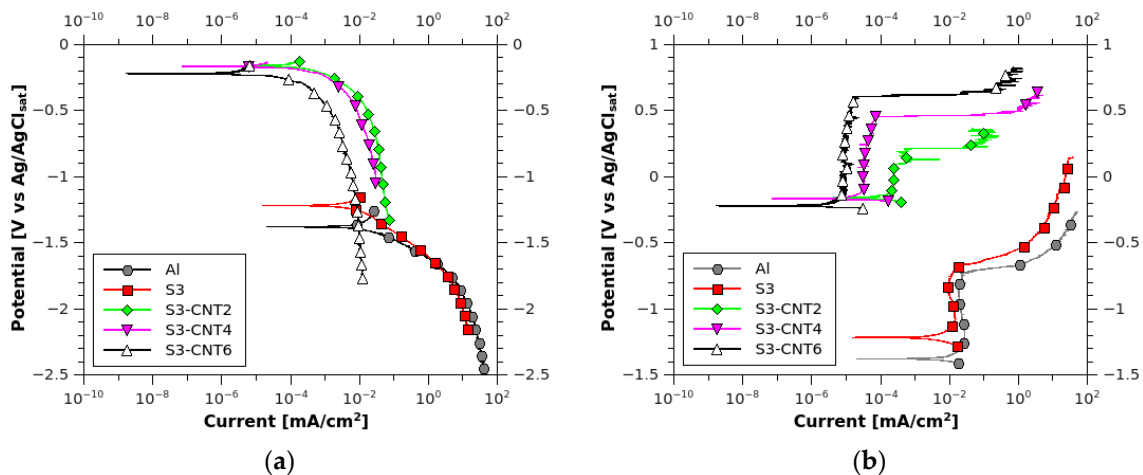

Figure 6. Potentiodynamic polarization curves in NaCl 3.5 wt.% solution for CNT silane coating for (**a**) cathodic branch (**b**) anodic branch. Bare aluminum and pure silane coating were also added as references.

At first, relevant considerations can be argued assessing the shifting of the open circuit potential (OCP), identifiable by the cusps of the curve, depending on surface coating deposition. The bare aluminum alloy sample evidences an OCP (also known as free corrosion potential) of ~−1.380 V versus Ag/AgCl$_{sat}$. This low corrosion potential, although not typical, was observed for some aluminum alloys [43]. In particular, Linardi et al. [44] evidenced, on Al6061 alloy, corrosion potential values at about −1.500 V vs. Ag/AgCl in a neutral deaerated solution.

A slight increase of about 0.150 V in the free corrosion potential can be observed in the presence of the pure silane coating (AS3), while the addition of the MWCNT filler in the silane matrix significantly affected the OCP. Samples coated with a composite CNT-silane film showed a corrosion potential (ranging between −0.160 V and −0.220 V vs. Ag/AgClsat) that is nobler than the bare aluminum one. In particular, the noblest potential (−0.160 V vs. Ag/AgClsat) was exhibited by the AS3-CNT2 specimen, characterized by 0.2 wt.% filler content. This result is due to the coupled action of the protective capacity of the coating and the improved electrical conductivity of the coating due to CNT addition.

The analysis of the cathodic branch of the potentiodynamic curves gives us further information about coating corrosion performance (Figure 6a). Examining the evolution of the cathodic curves, two cathodic trends due to oxygen or hydrogen reduction can be distinguished. The oxygen reduction reaction takes place at more noble potential. The curve is characterized by an abrupt decrease at decreasing potential exhibiting a vertical asymptote. This indicates a limit current density controlled by oxygen diffusion phenomena. Instead, the hydrogen evolution is the dominating reduction reaction only at less noble potentials, more evident on AS3 and bare aluminum surfaces [45]. The Tafel slope of the cathodic branch is 0.145 V/dec quite similar to the water reduction values, 0.140 to 0.160 V/dec, reported in the literature for aluminum alloys [43,46]. A very similar behavior was observed for pure silane-coated samples. The CNT-based coatings exhibit cathodic current density about three order of magnitude lower than bare aluminum substrate. This behavior is mainly related to the barrier action of the coating that limits the interaction of the aluminum surface with the electrolyte only in correspondence to local defects of the coating itself [47]. Moreover, the silane matrix is able to interact with the metal substrate generating covalent Al-O-Si bonds hindering the formation of

active adsorption sites on the metal surface [48]. Furthermore a depressed hydrogen reduction can be observed (AS3-CNT6 sample), to be ascribed probably to an increased hydrogen overpotential on CNT on the silane coating that shifted the cathodic hydrogen evolution curve at lower current [49]. Table 2 summarizes corrosion currents and open circuit potentials for all batches.

Table 2. Comparison of corrosion current and open circuit potentials for all batches.

Code	I_{corr} (mA/cm^2)	E_{corr} (V vs. Ag/AgCl$_{sat}$)
Al	1.0×10^{-2}	−1.380
AS3	0.8×10^{-2}	−1.210
AS3-CNT2	2.0×10^{-4}	−0.160
AS3-CNT4	3.0×10^{-4}	−0.190
AS3-CNT6	1.0×10^{-5}	−0.220

The comparison of the anodic curves of all samples leads to a better evaluation of the passivation behavior and resistance to local corrosion onset (Figure 6b). The bare aluminum exhibited an anodic branch with an evident passive region in the potential range −1.400–0.700 V vs. Ag/AgCl$_{sat}$ with a passivation current of about 2.0×10^{-2} mA/cm^2. Above −0.700 V, according to the literature, a breakdown of the passive film (identifiable by the abrupt increase in the anodic current density) takes place [43].

The pure silane coating showed an almost similar trend with a slightly higher OCP. Analogously, a slightly more noble breakdown potential than bare aluminum was also observed. Confirming the slight improvement in the surface corrosion stability induced by silane coating deposition, the passive region is characterized by a slightly lower anodic passivation current density (1.0×10^{-2} mA/cm^2).

A significant modification of the anodic branch of the curve can be noticed for the silane coatings filled with carbon nanotubes. All curves are characterized by a significantly lower anodic current density (about 3 orders of magnitude between 1.0×10^{-5} and 2.0×10^{-4} mA/cm^2) and breakdown potential much more noble than the base metal.

As the CNT content increases, the protective action of the coating becomes increasingly effective. In particular, the most effective anti-corrosive properties are found for the AS3-CNT6 specimen that exhibited a passivation current density of approximately 1.0×10^{-5} mA/cm^2 and a breaking potential of 0.620 V/AgAgCl$_{sat}$.

This indicates that the addition of CNT filler leads to obtaining a more electrochemically stable coating, able to preserve the aluminum substrate from local corrosion up to high potentials. The increase in the anti-corrosive properties observed for the CNT composite coatings can be related to the synergistic contribution of different factors such as the increase in barrier properties and hydrophobic behavior.

Indeed, with regard to the first factor, the CNT filler in the hybrid organic–inorganic silane matrix leads to a thicker and less porous protective film, thereby enhancing its barrier properties [50,51].

Moreover, CNTs embedded in the silane matrix influences the electrochemical surface interaction with water, because of the noticeable super-hydrophobic behavior of the sol-gel composite coating [52] and the consequent reduction of permeability and diffusivity of corrosive species [34,41]. Furthermore, the super-hydrophobic behavior of the CNT-based coatings limits the electrochemical reactivity of the surface in the electrolyte [53] by hindering the interaction with water.

Summarizing, this induced a relevant increase of OCP in all CNT-based coatings. Furthermore, All the composite coating exhibited very effective protective performances compared to pure silane one (AS3). In particular, the lowest corrosion current was observed on coating with the highest carbon nano-tube content (AS3-CNT6). This coating showed also the higher breakdown potential.

3.5. EIS Analysis

Impedance spectroscopy analysis was performed to provide further information on the composite coating properties and structure. Figure 7 displays the impedance spectra for the samples coated with

different CNT amount just after immersion in the 3.5 wt.% NaCl solution. For comparison purposes, the unfilled coating and bare aluminum samples are also reported. As expected, the coated samples have an impedance modulus almost higher than bare aluminum one, along the entire frequency range (with highest magnitude for sample AS3-CNT2).
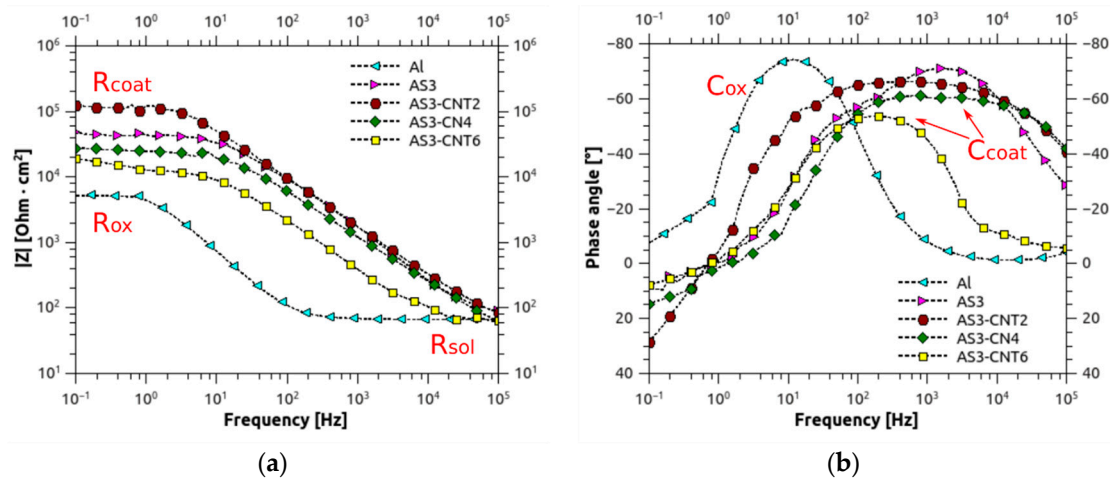

Figure 7. Bode plot of impedance modulus (**a**) and phase angle (**b**) of CNT filled and unfilled silane coating after 0 h of immersion in NaCl 3.5 wt.% solution.

By evaluating the phase angle plot in Figure 7b it is possible to identify a single time constants for all batches. For silane-based coating the time constant can be identified at high frequency ($\sim 10^2$–10^4 Hz), in correspondence of the phase angle peak, shifting toward lower frequency values as CNT content increases. This trend is typical of the capacitive behavior of insulating protective coating [54], C_{coat}. Instead, the bare aluminum sample, Al, exhibits a peak in the phase angle at low frequencies ($\sim 10^1$ Hz) related to the aluminum oxide layer [55], C_{ox}.

A plateau at low frequencies characterizes all curves in the impedance modulus vs. frequency plot (Figure 7a). The plateau in the bare aluminum spectrum is related to the thin aluminum oxide surface, R_{ox} ($\sim 5.6 \times 10^3$ $\Omega \cdot cm^2$ at 10^{-1} Hz) (the added R_{ox} value was identified as the impedance modulus magnitude at low frequency). The silane-based coated samples exhibit a larger plateau at higher magnitude of the impedance modulus (|Z|). In particular, the |Z| can be considered almost constant in the range ($\sim 10^{-1}$–10^1 Hz). This plateau at medium frequency is related to the resistive pore contribution of the CNT-silane coating, R_{coat}, [41]. The value of R_{coat} varies at increasing filler content.

At low carbon nanotube content the R_{coat} value increases. Afterward at large amount of CNT filler this value decreases becoming lower than silane sample one. The AS3-CNT2 sample showed the highest impedance values, about half an order of magnitude greater than the AS3-CNT6 one. The relatively reduced impedance of the AS3-CNT6 can be due to its irregular morphology. However, all sol-gel composite coatings show an impedance modulus at low frequencies always higher than the bare aluminum, confirming a beneficial protective action of the coating.

A less relevant difference among the |Z| magnitude of the silane coatings can be progressively observed at increasing frequencies where the composite coatings show a typical capacitive behavior, congruently to literature results [49], and as confirmed by the reduced phase angle that approaches to $-60°$ (Figure 7b).

This behavior, observed for all coated samples, can be related to the barrier action of the composite layer to electrolyte diffusion, indicating that all composite mixtures can offer a suitable protective action of the metal substrate. At low immersion times, this behavior can be mainly influenced by the synergistic action of porosity, barrier capability, or thickness. Considering the quite similar thickness of the coatings, it can be argued that CNT filler plays a relevant role in the anti-corrosion barrier properties of the coating.

The anti-corrosion effect of CNT addition in silane layer can be related to the synergistic action of several factors. Because of the large longitudinal vs. cross section ratio the carbon nanotubes are able to fill cracks and pores that naturally are generated during the curing process e.g., because of solvent evaporation, or matrix crosslinking [36]. This leads to a low coating permeability with subsequent good corrosion protective performances compared to the unfilled one. Furthermore, because of the suitable interfacial adhesion between composite coating constituents the protective layer is more compact exalting the barrier capabilities of the coating [33]. This allows slowing down the diffusion of aggressive species through the coating coupled to very limited and tortuous preferential diffusion pathways. At the same time the enhanced surface hydrophobicity hinders the water diffusion and exalts the anti-corrosion performance of the CNT coating compared to unfilled AS3 batch [56]. These beneficial effects are more evident in the nanocomposite coating with low CNT filler content where a relevant increase on impedance in a large frequency range was observed.

Conversely, at high CNT content (AS3-CNT6 batch) the EIS spectrum exhibited an almost lower impedance modulus magnitude. This behavior can be related to the triggering of partial agglomeration phenomena of the nanofiller that increased the water permeability [57]. Besides, a relevant role can be due the dielectric properties of the CNT coatings. The capacitive contribution can be influenced by the dielectric properties of the conductive carbon nanotube [58]. In particular, the addition of the conductive CNT filler in the insulating silane matrix involves a modification of the dielectric response of the material at high frequencies. The conductivity of the material leads to an increase in the dielectric constant, ε, with increased MWCNT loading [59]. Considering that the coating capacity, C, can be expressed as:

$$C = \varepsilon \varepsilon_0 A/d \tag{1}$$

where ε and ε_0 are the coating and vacuum dielectric constant (constant equal to 8.854×10^{-12} C/V·m), respectively, A and d are the coating area and thickness, respectively. The capacitance is directly proportional to ε value. Therefore, an increase of this parameter leads to a proportional increase of coating capacitance with subsequent shift of the EIS spectrum toward lower frequencies [49]. Analogous consideration can be argued for coating resistance modification at low frequency due to conductive filler addition.

In order to assess the evolution of the protective behavior of the coating during time, the EIS measurements were performed at increasing immersion time in the NaCl solution.

As reference, the evolution of impedance modulus and phase angle Bode plots at increasing immersion time of AS3-CNT6 coating, up to 72 h, is reported in Figure 8a,b, respectively.
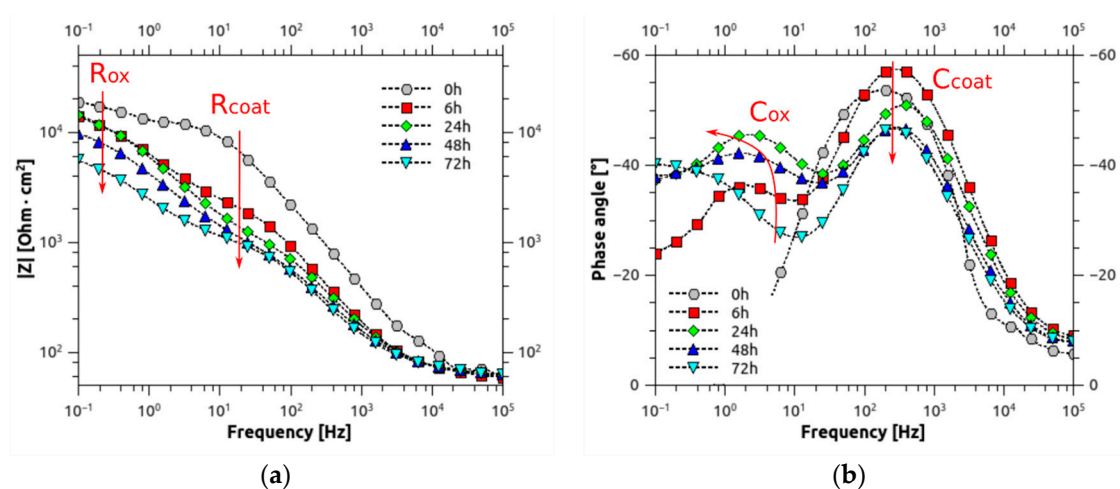

Figure 8. Bode plot of impedance modulus (**a**) and phase angle (**b**) of AS3-CNT6 batch at increasing immersion time.

Because of immersion in NaCl solution a significant change in the impedance trend takes place (Figure 8a). After 6 h, a wide depression of the impedance curve occurred. The impedance modulus suffered a decrease in magnitude in a large range of impedance. In particular, there was an abrupt decrease of |Z| at the medium frequencies of about 1 decade. This behavior is coupled to relevant changes also in phase angle (Figure 8b). The phase angle peak at about 10^2–10^3 Hz, progressively moves toward lower values of phase angle, while, at the same time, the formation of a secondary wide peak at about 10^0–10^1 Hz can be observed.

Structurally, two layers can represent the coating-substrate system: the outermost layer is the CNT-silane composite film. It has a very complex structure and morphology related to the chemical interaction among silane molecules, conductive carbon nanotubes and the substrate. The inner layer is related to the thin oxide film on the aluminum alloy surface. Therefore, the first time constant, identified at medium-high frequency can be related to the outer composite film (C_{coat}). Instead, the time constant at low frequency can be related to the electrochemical reactions at the aluminum surface and oxide film (C_{ox}).

In particular, this second peak shows a progressive increase in height and translation at lower frequencies. This is attributable to the water diffusion through the coating (from 6 h to 48 h immersion, as confirmed by the reduction of the phase angle) which reaches the metal surface triggering corrosion reactions on the aluminum surface (the secondary time constant peak at very low frequency after 72 h) [56].

These considerations are also confirmed by the significant |Z| value reduction at middle frequencies after few hours (6 h) of immersion in chloride solution (Figure 8a). This behavior is ascribed to a progressive reduction of the coating pore resistance, R_{coat}, and increase of the CNT-silane film capacity because of the water diffusion in the composite [60]. The variation of this contribution is relevant in the first stages of the aging test and decreases at increasing immersion time.

Conversely, the impedance modulus at low frequencies does not change significantly in the first stages of immersion. After the water penetrates through the coating and reaches the substrate, a more significant variation of the impedance modulus at low frequencies occurs. This phenomenon is particularly relevant after 48 h–72 h of immersion in the saline solution.

However, the protective properties of the composite coating (also after longest immersion time) are still acceptable, considering that the degradation phenomenon is in its initial stage. Similar behavior, although showing a different sensitivity to immersion time, was also found for the other batches (not reported here for sack of brevity).

Useful information concerning the anticorrosion performances of CNT-silane coatings can be acquired comparing the Bode plots of all samples after 72 h immersion time (Figure 9).
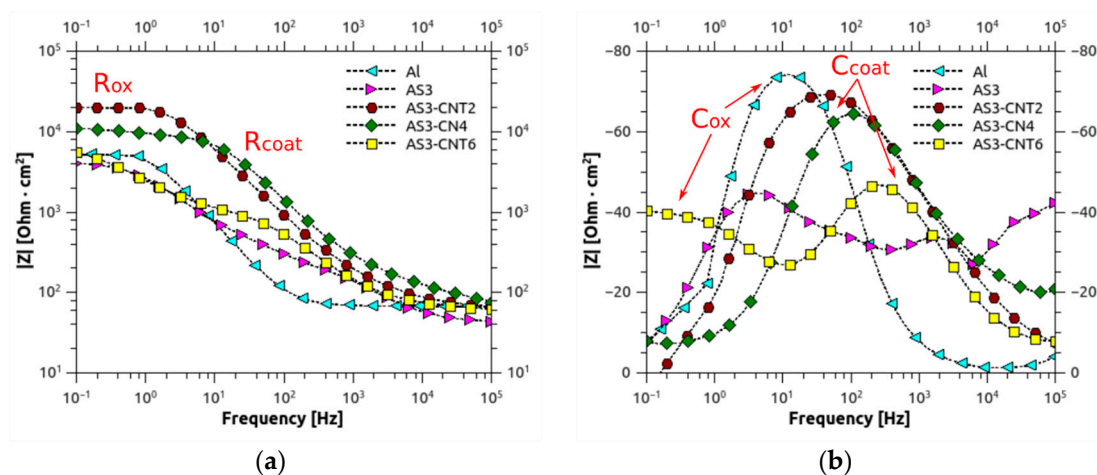

(a)   (b)

Figure 9. Bode plot of impedance modulus (**a**) and phase angle (**b**) of CNT filled and unfilled silane coating after 72 h of immersion in NaCl 3.5 wt.% solution.

The |Z| (Figure 9a) for AS3-CNT6 decreased significantly because of aging condition indicating a limited durability of this coating formulation in 3.5 wt.% NaCl solution. Probably because of the large agglomeration areas (Figure 2) the electrolyte penetrates through the coating and reached the metal substrate favoring the activation of corrosion phenomena at the interface. For this batch the observed impedance modulus magnitude at 0.1 Hz is quite similar to bare aluminum one. Instead, a more effective protective property is preserved by AS3-CNT2 and AS3-CNT4 coatings, as confirmed by the still higher |Z| value at low frequency. These considerations are confirmed by the evolution of phase angle, reported in Figure 9b.

For all sample a significant reduction of the phase angle in the whole frequency range occurred. For all batches the time constant, due to water diffusion in the nanocomposite coating, shift toward medium frequency. The batches lose their capacitive protective behavior (high phase angle at high frequency) and the phase angle in this range of frequency suffered a relevant decrease. In the low frequency range the trend at increasing CNT content shows the growth of a new time constant, as observed for AS3-CNT6 batch (Figure 8) ascribed to the triggering of corrosion phenomena due to the water permeation at the coating/substrate interface by the preferential pathways constituted by defects or pinholes [61].

By summarizing, it can be asserted that prolonged immersion in NaCl solution caused a progressive degradation of the CNT composite coatings, however, the formulations with lower nanotube content still showed an acceptable barrier action preserving the metal substrate from corrosion phenomena.

The hydrophobic behavior of the composite coatings certainly makes it possible to amplify the anti-corrosive action but does not represent the main driving force of the protective phenomenon. The surface properties act synergistically with the barrier action leading to increase in the durability of the layer with respect to the unfilled silane film.

These results, compatible and in some extent more promising than that reported in the literature on similar systems, represent a stimulus for future developments. This activity will be aimed to investigate in more details the mechanisms that oversee the degradation of the coatings in order to maximize their performance in the medium term to extend their potential application field.

4. Conclusions

In this work, a sol-gel N-propyl-trimethoxy-silane filled with different amount of multi-wall carbon nanotubes was deposited on an AA6061 aluminum alloy in order to improve the corrosion protection in chloride environment for marine application. SEM analysis showed an almost uniform morphology of the nanocomposite coating with 0.4% CNT. Coatings with lower or higher CNT filler content were characterized by heterogeneities or agglomeration, respectively. Pull-off and tape peel tests clarified the relevant cohesive and adhesive properties of the coating with the substrate. In particular, the pull-off strength ranged in 0.82–1.17 MPa for AC2-CNT6 and AS3-CNT2 batches, respectively.

The corrosion resistance of the metal substrate in NaCl 3.5 wt.% electrolyte solution was improved due to the CNT-based coating deposition. An acceptable stability in electrochemical impedance spectroscopy measurements was observed until three days of immersion in the chloride solution. AS3-CNT2 and AS3-CNT4 batches showed the higher electrochemical stability during immersion tests in chloride environment. In potentiodynamic polarization tests, a decrease of corrosion current of at least two order of magnitude was observed for all nanocomposite-coated samples. Furthermore, a shift of the breakdown potential to very noble potential was observed. The best results were observed on the AS3-CNT6 sample which evidenced a passivation current density of approximately 1.0×10^{-5} mA/cm^2 and a breaking potential of 0.620 V/AgAgCl$_{sat}$. The anticorrosion capability of this class of coating was ascribed to a synergistic action of several contributions. The coating increases its barrier properties because of CNT filler. Furthermore, a hydrophobic nature of the surface was exalted. The water contact angle on the unfilled silane coating increased from 90.2° to 160.3° by incorporating 0.6 wt.% of MWCNTs indicating considerable improvement in the hydrophobic property. Thus, the incorporation of CNT filler induced the increase of the hydrophobicity of the aluminum substrate, which positively

affected its corrosion resistance. Indeed, all the CNT films showed an improved corrosion protection for the aluminum alloy.

References

1. Deflorian, F.; Rossi, S.; Fedel, M. Organic coatings degradation: Comparison between natural and artificial weathering. *Corros. Sci.* **2008**, *50*, 2360–2366. [CrossRef]
2. Fihri, A.; Bovero, E.; Al-Shahrani, A.; Al-Ghamdi, A.; Alabedi, G. Recent progress in superhydrophobic coatings used for steel protection: A review. *Colloids Surf. A Physicochem. Eng. Asp.* **2017**, *520*, 378–390. [CrossRef]
3. Bayer, I.S. Superhydrophobic Coatings from Ecofriendly Materials and Processes: A Review. *Adv. Mater. Interfaces* **2020**, *7*, 2000095. [CrossRef]
4. Salehikahrizsangi, P.; Raeissi, K.; Karimzadeh, F.; Calabrese, L.; Proverbio, E. Highly hydrophobic Ni-W electrodeposited film with hierarchical structure. *Surf. Coat. Technol.* **2018**, *344*, 626–635. [CrossRef]
5. Salehikahrizsangi, P.; Raeissi, K.; Karimzadeh, F.; Calabrese, L.; Patane, S.; Proverbio, E. Erosion-corrosion behavior of highly hydrophobic hierarchical nickel coatings. *Colloids Surfaces A Physicochem. Eng. Asp.* **2018**, *558*, 446–454. [CrossRef]
6. Boyer, Q.; Duluard, S.; Tenailleau, C.; Ansart, F.; Turq, V.; Bonino, J.P. Functionalized superhydrophobic coatings with micro-/nanostructured ZnO particles in a sol–gel matrix. *J. Mater. Sci.* **2017**, *52*, 12677–12688. [CrossRef]
7. Zhang, X.; Zhu, W.; He, G.; Zhang, P.; Zhang, Z.; Parkin, I.P. Flexible and mechanically robust superhydrophobic silicone surfaces with stable Cassie-Baxter state. *J. Mater. Chem. A* **2016**, *4*, 14180–14186. [CrossRef]
8. Batalha Leoni, G.; de Freitas, D.S.; Ponciano Gomes, J.A.C.; Brasil, S.L.D.C. Multivariable analysis of electrodeposited silane based superhydrophobic coatings for corrosion protection of carbon steel. *J. Sol-Gel Sci. Technol.* **2020**, *94*, 695–707. [CrossRef]
9. Rioboo, R.; Demnati, I.; Amin Ali, M.; Sevkan, R.; De Coninck, J. Superhydrophobicity of composite surfaces created from polymer blends. *J. Colloid Interface Sci.* **2020**, *560*, 596–605. [CrossRef]
10. Yu, H.B.; Li, R.F. Preparation and properties of biomimetic superhydrophobic composite coating. *Surf. Eng.* **2016**, *32*, 79–84. [CrossRef]
11. Lu, Z.; Xu, L.; He, Y.; Zhou, J. One-step facile route to fabricate functionalized nano-silica and silicone sealant based transparent superhydrophobic coating. *Thin Solid Films* **2019**, *692*, 137560. [CrossRef]
12. Ghosal, A.; Iqbal, S.; Ahmad, S. NiO nanofiller dispersed hybrid Soy epoxy anticorrosive coatings. *Prog. Org. Coat.* **2019**, *133*, 61–76. [CrossRef]
13. Selim, M.S.; Yang, H.; Wang, F.Q.; Fatthallah, N.A.; Li, X.; Li, Y.; Huang, Y. Superhydrophobic silicone/SiC nanowire composite as a fouling release coating material. *J. Coat. Technol. Res.* **2019**, *16*, 1165–1180. [CrossRef]
14. Song, H.J.; Shen, X.Q.; Meng, X.F. Superhydrophobic surfaces produced by carbon nanotube modified polystyrene composite coating. *J. Dispers. Sci. Technol.* **2010**, *31*, 1465–1468. [CrossRef]
15. Men, X.H.; Zhang, Z.Z.; Yang, J.; Wang, K.; Jiang, W. Superhydrophobic/superhydrophilic surfaces from a carbon nanotube based composite coating. *Appl. Phys. A Mater. Sci. Process.* **2010**, *98*, 275–280. [CrossRef]
16. Sethi, S.K.; Manik, G. Recent Progress in Super Hydrophobic/Hydrophilic Self-Cleaning Surfaces for Various Industrial Applications: A Review. *Polym.-Plast. Technol. Eng.* **2018**, *57*, 1932–1952. [CrossRef]
17. Vazirinasab, E.; Jafari, R.; Momen, G. Application of superhydrophobic coatings as a corrosion barrier: A review. *Surf. Coat. Technol.* **2018**, *341*, 40–56. [CrossRef]
18. Nguyen-Tri, P.; Tran, H.N.; Plamondon, C.O.; Tuduri, L.; Vo, D.V.N.; Nanda, S.; Mishra, A.; Chao, H.P.; Bajpai, A.K. Recent progress in the preparation, properties and applications of superhydrophobic nano-based coatings and surfaces: A review. *Prog. Org. Coat.* **2019**, *132*, 235–256. [CrossRef]

19. Bakhsheshi-Rad, H.R.; Abdellahi, M.; Hamzah, E.; Daroonparvar, M.; Rafiei, M. Introducing a composite coating containing CNTs with good corrosion properties: Characterization and simulation. *RSC Adv.* **2016**, *6*, 108498–108512. [CrossRef]

20. Shoujie, L.; Hejun, L.; Leilei, Z.; Shaoxian, L.; Lina, P. The corrosion properties of carbon nanotubes-reinforced apatite composite coating on carbon/carbon composite by a double in situ process. *Surf. Eng.* **2019**, *35*, 96–101. [CrossRef]

21. Kausar, A. Corrosion Protection Behavior of Carbon Nanotube - based Nanocomposite. *Am. J. Environ. Sci. Technol.* **2019**, *3*, 22–29.

22. Peitao, G.; Mingyang, T.; Chaoyang, Z. Tribological and corrosion resistance properties of graphite composite coating on AZ31 Mg alloy surface produced by plasma electrolytic oxidation. *Surf. Coat. Technol.* **2019**, *359*, 197–205. [CrossRef]

23. Hussain, A.K.; Sudin, I.; Basheer, U.M.; Yusop, M.Z.M. A review on graphene-based polymer composite coatings for the corrosion protection of metals. *Corros. Rev.* **2019**, *37*, 343–363. [CrossRef]

24. Foyet, A.; Wu, T.H.; Kodentsov, A.; van der Ven, L.G.J.; de With, G.; van Benthem, R.A.T.M. Corrosion Protection and Delamination Mechanism of Epoxy/Carbon Black Nanocomposite Coating on AA2024-T3. *J. Electrochem. Soc.* **2013**, *160*, C159–C167. [CrossRef]

25. De Nicola, F.; Castrucci, P.; Scarselli, M.; Nanni, F.; Cacciotti, I.; De Crescenzi, M. Super-hydrophobic multi-walled carbon nanotube coatings for stainless steel Related content. *Nanotechnology* **2015**, *26*, 14570. [CrossRef]

26. Zhu, X.; Zhou, S.; Yan, Q.; Wang, S. Multi-walled carbon nanotubes enhanced superhydrophobic MWCNTs-Co/a-C:H carbon-based film for excellent self-cleaning and corrosion resistance. *Diam. Relat. Mater.* **2018**, *86*, 87–97. [CrossRef]

27. Zhou, S.; Zhu, X.; Ma, L.; Yan, Q.; Wang, S. Outstanding superhydrophobicity and corrosion resistance on carbon-based film surfaces coupled with multi-walled carbon nanotubes and nickel nano-particles. *Surf. Sci.* **2018**, *677*, 193–202. [CrossRef]

28. Canobre, S.C.; Almeida, D.A.L.; Polo Fonseca, C.; Neves, S. Synthesis and characterization of hybrid composites based on carbon nanotubes. *Electrochim. Acta* **2009**, *54*, 6383–6388. [CrossRef]

29. Serp, P.; Corrias, M.; Kalck, P. Carbon nanotubes and nanofibers in catalysis. *Appl. Catal. A Gen.* **2003**, *253*, 337–358. [CrossRef]

30. Deyab, M.A. Corrosion protection of aluminum bipolar plates with polyaniline coating containing carbon nanotubes in acidic medium inside the polymer electrolyte membrane fuel cell. *J. Power Sources* **2014**, *268*, 50–55. [CrossRef]

31. Khun, N.W.; Rincon Troconis, B.C.; Frankel, G.S. Effects of carbon nanotube content on adhesion strength and wear and corrosion resistance of epoxy composite coatings on AA2024-T3. *Prog. Org. Coat.* **2014**, *77*, 72–80. [CrossRef]

32. Hammer, P.; dos Santos, F.C.; Cerrutti, B.M.; Pulcinelli, S.H.; Santilli, C.V. Corrosion Resistant Coatings Based on Organic-Inorganic Hybrids Reinforced by Carbon Nanotubes. In *Recent Researches in Corrosion Evaluation and Protection*; Reza, S.R., Ed.; Intech: London, UK, 2012; pp. 117–142.

33. Liu, Y.; Cao, H.; Yu, Y.; Chen, S. Corrosion Protection of Silane Coatings Modified by Carbon Nanotubes on Stainless Steel. *Int. J. Electrochem. Sci.* **2015**, *10*, 3497–3509.

34. Jeeva Jothi, K.; Palanivelu, K. Synergistic effect of silane modified nanocomposites for active corrosion protection. *Ceram. Int.* **2013**, *39*, 7619–7625. [CrossRef]

35. Montemor, M.F.; Ferreira, M.G.S. Analytical characterisation and corrosion behaviour of bis-aminosilane coatings modified with carbon nanotubes activated with rare-earth salts applied on AZ31 Magnesium alloy. *Surf. Coat. Technol.* **2008**, *202*, 4766–4774. [CrossRef]

36. Nezamdoust, S.; Seifzadeh, D.; Rajabalizadeh, Z. PTMS/OH-MWCNT sol-gel nanocomposite for corrosion protection of magnesium alloy. *Surf. Coat. Technol.* **2018**, *335*, 228–240. [CrossRef]

37. Piperopoulos, E.; Calabrese, L.; Mastronardo, E.; Proverbio, E.; Milone, C. Synthesis of reusable silicone foam containing carbon nanotubes for oil spill remediation. *J. Appl. Polym. Sci.* **2018**, *135*, 46067. [CrossRef]

38. Messina, G.; Modafferi, V.; Santangelo, S.; Tripodi, P.; Donato, M.G.; Lanza, M.; Galvagno, S.; Milone, C.; Piperopoulos, E.; Pistone, A. Large-scale production of high-quality multi-walled carbon nanotubes: Role of precursor gas and of Fe-catalyst support. *Diam. Relat. Mater.* **2008**, *17*, 1482–1488. [CrossRef]

39. Milone, C.; Shahul Hameed, A.R.; Piperopoulos, E.; Santangelo, S.; Lanza, M.; Galvagno, S. Catalytic wet air oxidation of p-coumaric acid over carbon nanotubes and activated carbon. *Ind. Eng. Chem. Res.* **2011**, *50*, 9043–9053. [CrossRef]

40. Calabrese, L.; Bonaccorsi, L.; Caprì, A.; Proverbio, E. Adhesion aspects of hydrophobic silane zeolite coatings for corrosion protection of aluminium substrate. *Prog. Org. Coat.* **2014**, *77*, 1341–1350. [CrossRef]

41. Akbarzadeh, S.; Naderi, R.; Mahdavian, M. Fabrication of a highly protective silane composite coating with limited water uptake utilizing functionalized carbon nano-tubes. *Compos. Part B Eng.* **2019**, *175*, 107109. [CrossRef]

42. Calabrese, L.; Bonaccorsi, L.; Caprì, A.; Proverbio, E. Effect of silane matrix composition on performances of zeolite composite coatings. *Prog. Org. Coat.* **2016**, *101*, 100–110. [CrossRef]

43. Gerhard Kreysa, M.S. *Corrosion Handbook, Corrosive Agents and Their Interaction with Materials, Volume 7, Sodium Chloride*; Wiley VCH: Weinheim, Germany, 2007; ISBN 9783527311231.

44. Linardi, E.; Haddad, R.; Lanzani, L. Stability Analysis of the Mg2Si Phase in AA 6061 Aluminum Alloy. *Procedia Mater. Sci.* **2012**, *1*, 550–557. [CrossRef]

45. Calabrese, L.; Bonaccorsi, L.; Proverbio, E. Corrosion protection of aluminum 6061 in NaCl solution by silane-zeolite composite coatings. *J. Coat. Technol. Res.* **2012**, *9*, 597–607. [CrossRef]

46. Vargel, C. *Corrosion of Aluminium*; Elsevier: Amsterdam, The Netherlands, 2004; ISBN 9780080444956.

47. Calabrese, L.; Bonaccorsi, L.; Caprì, A.; Proverbio, E. Assessment of hydrophobic and anticorrosion properties of composite silane–zeolite coatings on aluminum substrate. *J. Coat. Technol. Res.* **2016**, *13*, 287–297. [CrossRef]

48. van Ooij, W.J.; Zhu, D.; Stacy, M.; Seth, A.; Mugada, T.; Gandhi, J.; Puomi, P. Corrosion protection properties of organofunctional silanes—An overview. *Tsinghua Sci. Technol.* **2005**, *10*, 639–664. [CrossRef]

49. Calabrese, L.; Bonaccorsi, L.; Caprì, A.; Proverbio, E. Electrochemical behavior of hydrophobic silane–zeolite coatings for corrosion protection of aluminum substrate. *J. Coat. Technol. Res.* **2014**, *11*, 883–898. [CrossRef]

50. Chen, F.; Zhang, Y.; Zhang, Y. Effect of Graphene on Micro-Structure and Properties of MAO Coating Prepared on Mg-Li Alloy. *Int. J. Electrochem. Sci.* **2017**, *12*, 6081–6091. [CrossRef]

51. Zhou, C.; Lu, X.; Xin, Z.; Liu, J.; Zhang, Y. Polybenzoxazine/SiO_2 nanocomposite coatings for corrosion protection of mild steel. *Corros. Sci.* **2014**, *80*, 269–275. [CrossRef]

52. Han, J.T.; Kim, S.Y.; Woo, J.S.; Lee, G.-W. Transparent, Conductive, and Superhydrophobic Films from Stabilized Carbon Nanotube/Silane Sol Mixture Solution. *Adv. Mater.* **2008**, *20*, 3724–3727. [CrossRef]

53. Sharma, V.; Goyat, M.S.; Hooda, A.; Pandey, J.K.; Kumar, A.; Gupta, R.; Upadhyay, A.K.; Prakash, R.; Kirabira, J.B.; Mandal, P.; et al. Recent progress in nano-oxides and CNTs based corrosion resistant superhydrophobic coatings: A critical review. *Prog. Org. Coat.* **2020**, *140*, 105512. [CrossRef]

54. Lasia, A. *Electrochemical Impedance Spectroscopy and Its Applications*; Springer: Berlin/Heidelberg, Germany, 2014; ISBN 9781461489337.

55. Huang, Y.; Shih, H.; Daugherty, J.; Mansfeld, F. Evaluation of the properties of anodized aluminum 6061 subjected to thermal cycling treatment using electrochemical impedance spectroscopy (EIS). *Corros. Sci.* **2009**, *51*, 2493–2501. [CrossRef]

56. Jeon, H.R.; Park, J.H.; Shon, M.Y. Corrosion protection by epoxy coating containing multi-walled carbon nanotubes. *J. Ind. Eng. Chem.* **2013**, *19*, 849–853. [CrossRef]

57. Vivar Mora, L.; Naik, S.; Paul, S.; Dawson, R.; Neville, A.; Barker, R. Influence of silica nanoparticles on corrosion resistance of sol-gel based coatings on mild steel. *Surf. Coat. Technol.* **2017**, *324*, 368–375. [CrossRef]

58. Poh, C.L.; Mariatti, M.; Noor, A.F.M.; Sidek, O.; Chuah, T.P.; Chow, S.C. Dielectric properties of surface treated multi-walled carbon nanotube/epoxy thin film composites. *Compos. Part B Eng.* **2016**, *85*, 50–58. [CrossRef]

59. Chang, J.; Liang, G.; Gu, A.; Cai, S.; Yuan, L. The production of carbon nanotube/epoxy composites with a very high dielectric constant and low dielectric loss by microwave curing. *Carbon* **2012**, *50*, 689–698. [CrossRef]

60. Song, D.; Yin, Z.; Liu, F.; Wan, H.; Gao, J.; Zhang, D.; Li, X. Effect of carbon nanotubes on the corrosion resistance of water-borne acrylic coatings. *Prog. Org. Coat.* **2017**, *110*, 182–186. [CrossRef]

61. Calabrese, L.; Proverbio, E. A brief overview on the anticorrosion performances of sol-gel zeolite coatings. *Coatings* **2019**, *9*, 409. [CrossRef]